ACS APPLIED MATERIALS & INTERFACES

Research Article

Cite This: ACS Appl. Mater. Interfaces 2019, 11, 40310−40319

www.acsami.org

Mechanistic Insights into the Effect of Polymer Regioregularity on the Thermal Stability of Polymer Solar Cells

Yu-Ching Huang,*[,†] Wei-Shin Liu,[‡,§] Cheng-Si Tsao,*[,∥,⊥] and Leeyih Wang*[,‡,§]

[†]Department of Materials Engineering, Ming Chi University of Technology, New Taipei City 24301, Taiwan

[‡]Institute of Polymer Science and Engineering, [§]Center for Condensed Matter Sciences, and [∥]Department of Materials Science and Engineering, National Taiwan University, Taipei 10617, Taiwan

[⊥]Institute of Nuclear Energy Research, Longtan, Taoyaun 32546, Taiwan

Supporting Information

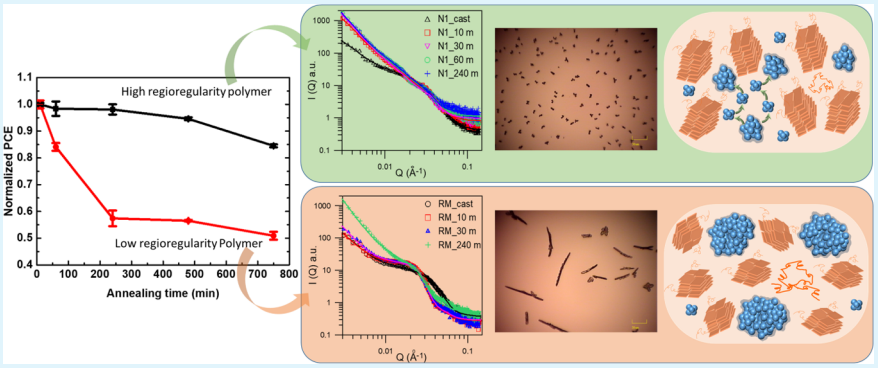

ABSTRACT: Thermal stability is a bottleneck toward commercialization of polymer solar cells (PSCs). The effect of PCBM aggregation on a multilength scale on the bulk-heterojunction (BHJ) structure, performance, and thermal stability of PSCs is studied here by grazing-incidence small- and wide-angle X-ray scattering. The evolution of hierarchical BHJ structures of a blend film tuned by regioregularity of polymers from the as-cast state to the thermally unstable state is systematically investigated. The thermal stability of PSCs with high polymer regioregularity values can be improved because of the good mutual interaction between polymer crystallites and fullerene aggregates. The insights obtained from this study provide an approach to manipulate the film structure on a multilength scale and to enhance the thermal stability of P3HT-based PSCs.

KEYWORDS: *polymer solar cell, thermal stability, PCBM aggregation, GISAXS, GIWAXS, bulk heterojunction, nanostructure*

INTRODUCTION

Polymer solar cells (PSCs) are the next generation of solar cells due to the advantages of low cost, low weight, mechanical flexibility, and easy manufacture.[1−3] However, there exists thermal stability problems, which hinder the future commercialization and applications of this technology. Previous studies have reported that the thermal instability of PSCs results from a severe phase separation of the active layer, including aggregation of fullerene derivatives.[4,5] Therefore, several approaches were developed to suppress the microscale phase segregation induced by thermal degradation. These approaches adopt (1) control of the side chain or backbone of polymers,[6−8] (2) polymers with a high glass-transition temperature,[9−11] (3) photo-cross-linked or functionalized donor polymers,[12,13] etc. These approaches were reviewed in our previous study.[14] There are adverse problems caused by the above approaches. Disturbance of the conjugated polymer crystallization or hindrance to the fullerene diffusion and aggregation from the aggregation inhibitor could destroy the originally favorable bulk-heterojunction (BHJ) structure, and thus lower the desired device performance. These studies reported that the coalescence of the nanoscale BHJ domains leads to microscale phase segregation. In addition, our previous research revealed that phase-separation regimes on multilength scales (nanoscale, mesoscale, and macroscale) affect the thermal stability of PSCs. According to a quantitative analysis of the BHJ structure evolution, a mesoscale PCBM-rich/P3HT amorphous domain was proven to grow with annealing at 150 °C for a long time.[14] Although our previous study has pointed out phase separation on multilength scales, the knowledge on the mutual influence between fullerene aggregation and polymer crystallization at different scales during the thermal degradation period is still insufficient. To find a rational strategy for enhancing the thermal stability and cell performance, an in-depth understanding of the mechanism through which the donor and the acceptor components in the multilength-scale BHJ structure mutually interact during prolonged annealing is necessary. Many studies have focused on tuning the polymer crystallinity to improve the performance of P3HT-based PSCs. The polymer

Received: July 16, 2019
Accepted: October 9, 2019
Published: October 9, 2019

DOI: 10.1021/acsami.9b12482
ACS Appl. Mater. Interfaces 2019, 11, 40310−40319

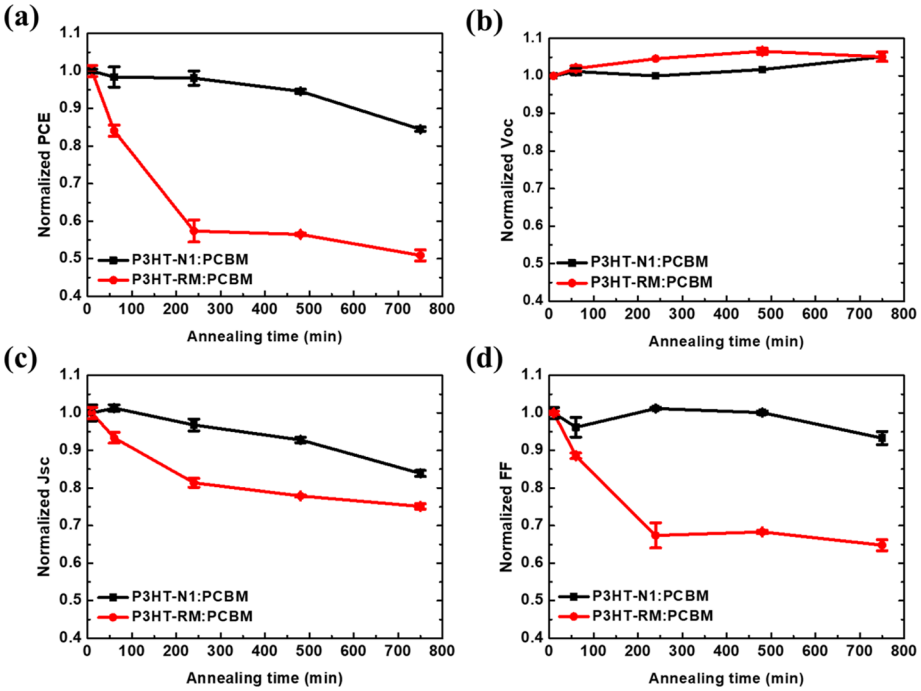

Figure 1. Variation of (a) V_{OC}, (b) J_{SC}, (c) FF, and (d) PCE of the P3HT-RM and -N1:PCBM devices with thermal annealing time at 150 °C.

crystallinity can be tuned by thermal annealing,[15] solvent annealing,[16] and solvent additive addition.[17] The effect of polymer regioregularity (RR) on the BHJ morphology and optoelectronic properties has also been demonstrated in previous literature.[18−21] However, these studies mainly focus on how morphological evolution affects the power conversion efficiency (PCE) of PSCs. The effects of the mutual interaction between P3HT and PCBM on multilength scales on the BHJ structure and thermal stability were seldom investigated. A previous research pointed out that the crystallinity of P3HT was very important to the formation of a thermally stable BHJ with PCBM.[22] They tuned the BHJ morphology by controlling the RR of P3HT, demonstrating that the RR of P3HT largely affects the thermal stability of PSCs. That study provided initial evidence that the mutual interaction between polymer and fullerene has a great impact on the thermal stability and BHJ nanostructure stability under prolonged annealing. It was broadly accepted that the thermally stable BHJ with PCBM is critical for enhancing the thermal stability of PSCs.

Grazing-incidence small- and wide-angle X-ray scattering (GISAXS and GIWAXS) have been considered as powerful techniques for studying the hierarchical BHJ morphology of PSCs.[23−26] Previous PSC studies reported that the phase-separated nanostructure, composed of (1) crystallization of the donor polymer, (2) aggregation of fullerene molecules into nanoscale clusters, and (3) an amorphous polymer/fullerene domain, forms an effective interpenetration network for charge separation at the polymer−fullerene interface and the subsequent charge transport.[23,24,27] This phase-separated BHJ structure is thermodynamically unstable and would kinetically degrade under prolonged thermal annealing or overheating. Current studies are limited to microscopic observations, focusing on the macro- or mesoscale segregation of the polymer and fullerene phases under prolonged thermal annealing. Our previous study[14] utilized concurrent GISAXS and GIWAXS measurements to quantitatively investigate the hierarchical structures and their evolution on the P3HT:PCBM solar cell from BHJ to thermally unstable structures. Our results demonstrated that the thermally unstable structure was closely related to the structural evolution at the meso- and macroscale. The phase-separation regimes of P3HT crystallization and fullerene aggregation at the nano- and mesoscale revealed were independent. Bis-PCBM molecules can manipulate the hierarchical structures to effectively stabilize the film morphology. It was demonstrated that GISAXS/GIWAXS can provide insight into the microscopic observation of the hierarchically complex structure. The information obtained is beyond the conventional understanding based on microscopy. There is, then, motivation to explore the formation, growth, and mutual interaction of donor and acceptor phases in the hierarchical evolution tailored by other factors.

In this paper, we reveal another mechanism for improving the thermal stability and performance of PSCs with an active layer of a blend of P3HT and PCBM by the control of multilength-scale PCBM aggregation. Concurrent GISAXS and GIWAXS were executed to characterize the evolution of the hierarchical structures of the P3HT:PCBM blend film with different polymer RRs from as-cast, optimal BHJ to finally unstable structures. The mechanism proposed here is based on polymer crystallization, PCBM aggregation, and mutual confinement between the polymer and PCBM phases. The mechanistic understanding can provide insight into the manipulation of multilength-scale BHJ structures and phase separation and their correlation for the improvement of thermal stability. This study presents more opportunities on finely tuned thermally stable BHJs with PCBM.

EXPERIMENTAL SECTION

Preparation and Characterization of P3HT:PCBM Blend Films. P3HT polymers with different regioregularities of 91.7 and 96.7%, were purchased from Rieke Metals and Grignard Metathesis, respectively. They were named P3HT-RM (low RR) and P3HT-N1 (high RR) samples, respectively. The measurement of RR for both polymers was performed using the NMR approach (Supporting Information, Figure S1). The active layer solution was prepared by

DOI: 10.1021/acsami.9b12482
ACS Appl. Mater. Interfaces 2019, 11, 40310−40319

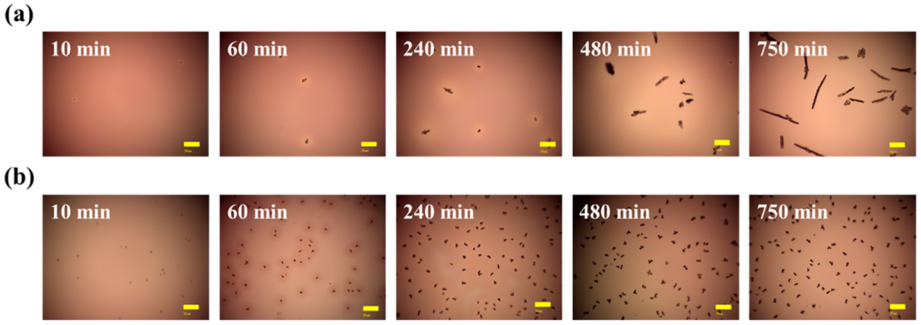

Figure 2. OM images of the (a) P3HT-RM:PCBM and (b) P3HT-N1:PCBM blend films annealed at 150 °C for 10, 60, 240, 480, and 750 min (scale bars: 50 μm).

blending 10 mg of P3HT and 8 mg of PCBM (as the acceptor) in 1 mL of CB. Two kinds of spin-cast active layers were prepared with P3HT-RM and P3HT-N1 polymers, respectively. The corresponding PSC devices were prepared with the conventional structure: glass/indium tin oxide (ITO)/poly(3,4-ethylenedioxythiophene):polystyrene sulfonate (PEDOT:PSS)/P3HT:PCBM/Ca/Al. For testing the thermal stability, various thermal annealing periods were performed at 150 °C for 10, 60, 240, 480, and 750 min before the Ca/Al cathode was deposited on the devices. Voltage−photocurrent (J−V) behaviors of the PSCs treated with different thermal annealing times were obtained under A.M. 1.5G conditions (100 mW cm^{-2}). The device area was defined by the electrode area of 1 × 0.1 cm^2. We also determined the hole and electron mobilities by using the space-charge-limited current measurements. The BHJ morphologies of the P3HT-N1:PCBM and P3HT-RM:PCBM thin films under the same thermal annealing treatments were observed using optical microscopy (OM) and transmission electron microscopy (TEM). The UV−visible absorption and photoluminescence (PL) behaviors of the corresponding P3HT/PCBM thin films were studied using a conventional spectrophotometer (Jasco V-670) and a photoluminescence spectrometer (Jobin Yvon Fluorolog-Tau-3), respectively. The incident photon-to-current conversion efficiency spectra were collected with a monochromator (Triax 180, Jobin Yvon).

Simultaneous GISAXS/GIWAXS Measurements for P3HT:PCBM Blend Films. The P3HT-RM and P3HT-N1:PCBM blend films for GISAXS/GIWAXS experiments were spin-cast on Si substrates (2 × 1 cm^2). Our previous results have confirmed that the P3HT:PCBM blend films exhibit almost the same scattering curves on either an Si/PEDOT:PSS substrate or an Si substrate. Therefore, we ignored the PEDOT:PSS effect on the scattering data herein.[23] The P3HT-N1:PCBM blend films were thermally annealed at 150 °C for 0, 10, 30, 60, 240, and 600 min. The P3HT-RM:PCBM films as the control or reference group were thermally annealed at 150 °C for 0, 10, 30, and 240 min. For quantitatively studying the influence of prolonged annealing on structural evolution, we conducted concurrent GISAXS and GIWAXS measurements at the 23A beamline station of the National Synchrotron Radiation Research Center in Taiwan, and we adopted the same instrument configuration and operation procedure reported previously.[14,23] One-dimensional (1D) GISAXS profiles were obtained by data reduction according to our previous literature.[14] The reduced 1D GISAXS data mainly covered the Yoneda peak for extracting the accurate information of the BHJ structure in the blend film.[28,29] In contrast, the out-of-plane direction is defined as the Z-direction, which is perpendicular to the film surface. The 1D GIWAXS profiles were reduced by taking a slice cake (polar angle (χ): 85−90° along the out-of-plane direction, Q_z, for the edge-on crystallites; χ: 0−5° along the in-plane direction, Q_x, for the face-on crystallites; χ: 0−90° to representatively include all P3HT crystallites with different orientations) from the 2D GIWAXS pattern to include the (100) diffraction spots from P3HT crystallites with different orientations.

RESULTS AND DISCUSSION

Thermal Stability of P3HT:PCBM Devices Treated with Prolonged Annealing. Figure 1 shows the temporal variations in the photovoltaic characteristics of devices based on the P3HT-RM:PCBM and P3HT-N1:PCBM blend films annealed at 150 °C for 10, 60, 240, 480, and 750 min. The photovoltaic characteristics and J−V curves of the corresponding devices are presented in the electronic Supplementary Information (Figure S2 and Table S1). Figure 1 illustrates that the PCE of P3HT-RM-based devices rapidly drops below 60% of the initial PCE (3.4%) after annealing for 200 min, showing the device's poor thermal stability. These results are consistent with those of our previous studies.[4,14] In contrast, the P3HT-N1-based devices show high thermal stability with 85% of the initial PCE (3.7%) at 720 min of prolonged annealing. V_{OC} is not sensitive to the thermal effect and remains constant during the prolonged annealing in both devices. In contrast, both J_{SC} and FF rapidly decay with increasing annealing time. The variation in FF with annealing time is the most critical factor that determines the thermal degradation of the two kinds of devices in this study. It is noteworthy that our results are different from those of the literature.[22] A previous study[22] reported that the PCE of devices with low-RR P3HT (91%) does not strongly decrease after thermal annealing at 150 °C for 300 min, but the PCE of devices based on a high-RR polymer (96%) decreases due to severe phase separation. The reason for this result is that micron-scale PCBM aggregation is not observed due to the use of low-RR P3HT. In our current study, however, we clarify that the micron-scale PCBM aggregation is not the most critical factor for thermal stability. For understanding this discrepancy, we studied the influence of PCBM aggregation on the thermal stability of PSCs through nanostructure analysis.

Structural Characterization and Properties of the Phase-Separated P3HT-XX:PCBM Blend Films. Both OM and TEM were employed to observe the morphological evolution with annealing time. Figure 2 shows the OM images of macrosized phase separation of both P3HT-RM and P3HT-N1:PCBM blend films annealed at 150 °C. The black dots in the images are identified as PCBM-rich clusters according to a previous study.[4] Both blend films reveal black dots as the annealing prolongs. Because of the large discrepancy between thermal stabilities, there are two evolution patterns of macrosize segregation. For the P3HT-RM-based blend films with poor thermal stability, the black dots nucleated, gradually grew in size and number, and finally developed (or aggregated) into large rod-like domains. In contrast, for the P3HT-N1-based blend films with high thermal stability, the size of the black dots remained small and only their quantity grew with the prolonged

DOI: 10.1021/acsami.9b12482
ACS Appl. Mater. Interfaces 2019, 11, 40310−40319

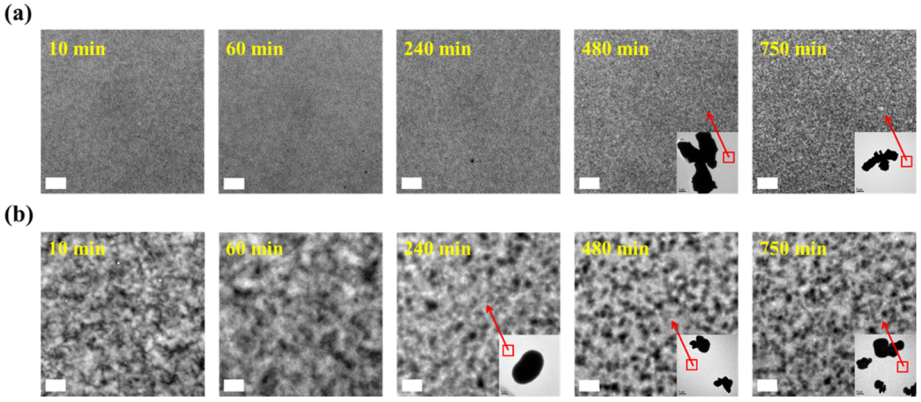

Figure 3. TEM micrographs of the (a) P3HT-RM:PCBM and (b) P3HT-N1:PCBM blend films annealed at 150 °C for 10, 60, 240, 480, and 750 min (scale bar: 1 μm). The insets display the corresponding position and black dots identified in OM observation.

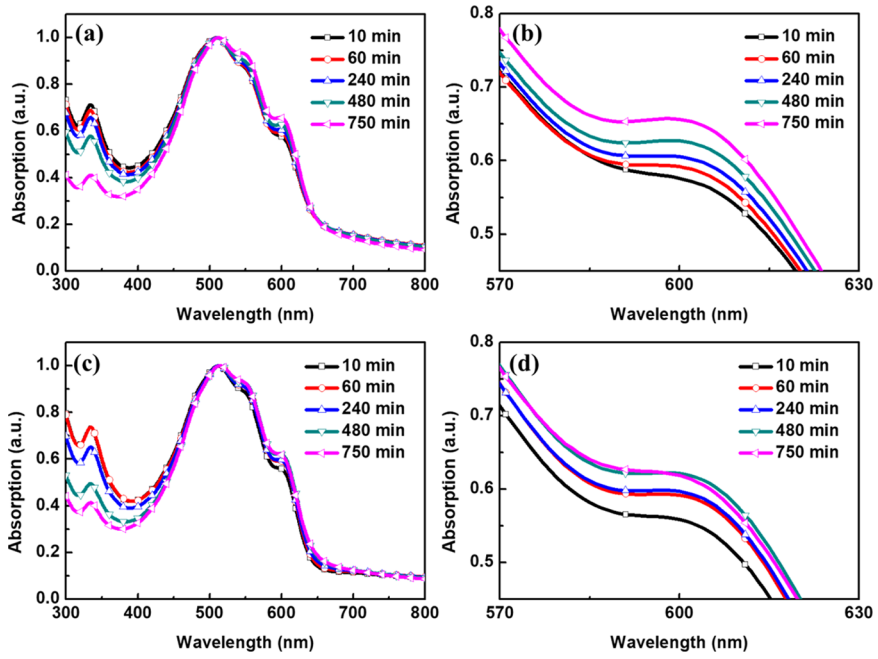

Figure 4. UV−vis absorption spectra of the (a, b) P3HT-RM:PCBM and (c, d) P3HT-N1:PCBM blend films treated at 150 °C for 10, 60, 240, 480, and 750 min.

annealing. In the previous literature,[22] they used low-RR P3HT to avoid PCBM aggregation. However, our results show that it is still possible to generate large PCBM aggregates after long-term thermal annealing even if we used the P3HT with a similar RR. This result implied that the RR of the polymer is not the only influencing factor in the phase-separation behavior of P3HT:PCBM under thermal treatment. However, it is beyond the research focus of this paper. In this study, we mainly focus on the mechanism through which the PSCs maintain good thermal stability even if large PCBM aggregates exist. This is different from the well-known facts, and we believe our current research can yield a further understanding of the mechanism of PSCs' thermal stability.

The TEM images in Figure 3 correspond to the featureless (almost no black aggregate) areas of the OM images; they show the morphological evolution at a smaller scale (around one order lower than the scale of the OM images). The bright and dark regions indicate P3HT-rich and PCBM-rich domains, respectively. The PCBM-rich domains of the P3HT-N1-based films significantly increase in number after t = 480 min. The sizes of the PCBM-rich domains remain stable and range from around 300−600 nm. The thermally stable behavior of domain size (hundreds of nanometers) is consistent with that of larger micron-sized dots in the OM images. The PCBM-rich domains of the P3HT-RM-based films cannot be visibly identified. The reasons may be the following: (1) the electron density contrast between phases is too weak and (2) the feature object is smaller than 100 nm, which is beyond the TEM resolution.

Figure 4 exhibits the absorption spectra of the P3HT-RM:PCBM and P3HT-N1:PCBM blend films annealed at 150 °C. The broad absorption peak at 515 nm (from the $\pi-\pi^*$ transition in the P3HT) for both blend films does not vary with annealing time. Therefore, we normalized the absorption spectra according to the peak at 515 nm. Figure 4b,d shows the absorption range from 570 to 630 nm, which is the absorption shoulder ascribed to the interchain stacking of P3HT. From the resolution of the spectra, we can find that the crystallinity of P3HT-RM gradually increased with the thermal annealing time. In contrast, the crystallinity of P3HT-N1 reached an initial saturation within 60 min; a further increase in crystallinity is

DOI: 10.1021/acsami.9b12482
ACS Appl. Mater. Interfaces 2019, 11, 40310−40319

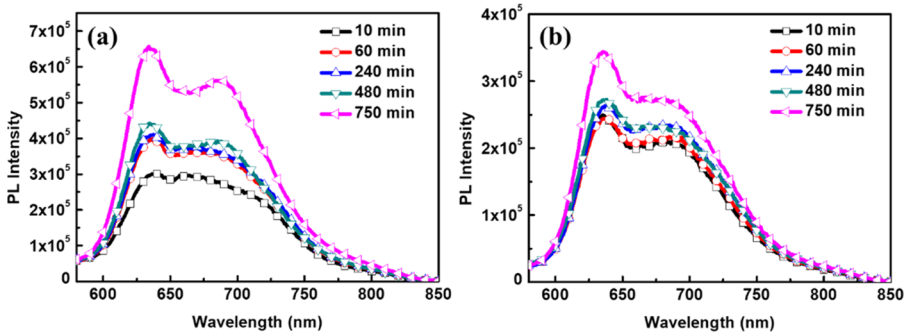

Figure 5. Photoluminescence spectra of the (a) P3HT-RM:PCBM and (b) P3HT-N1:PCBM blend films annealed at 150 °C for 10, 60, 240, 480, and 750 min.

shown after a longer annealing time (>480 min). It is worth noting that the use of UV−vis spectra to measure the crystallinity of the polymer is an indirect method, so it is not quite sensitive to the real crystallinity. Therefore, we use GIWAXS to better present the different crystallinity behaviors in the polymer blend films in the following study. In addition, the main absorption peaks at 330 nm (from the $\pi-\pi^*$ transition in PCBM) for both blend films consistently decay with annealing time. This decrease signifies that the segregation effect of micron-sized PCBM clusters on the scattering of incident light increases with annealing time, although both blend films have entirely different segregation patterns, as described above. Figure 5 shows the corresponding photoluminescence (PL) spectra of these annealed P3HT-RM:PCBM and P3HT-N1:PCBM blend films. With an increase in annealing time, the emission of P3HT-RM-based blend films increases significantly, implying that the formation of large micron-sized dots and their growth into rod-like aggregates significantly decrease the interfacial area between phases, and thus largely degrade the charge dissociation at the interface. In contrast, the emission of P3HT-N1-based blend films slightly increases with annealing time. This suggests that uniformly distributed PCBM-rich domains (around hundreds of nanometers; in the TEM images) and micron-sized dots (>10 μm; in the OM images) with thermally stable sizes could cause lower charge dissociation loss at the interface between two phases compared to the P3HT-RM-based blend films.

Evolution of Multilength-Scale BHJ Structures of Thermally annealed P3HT-XX:PCBM Blend Films: Quantitative GISAXS/GIWAXS Analysis. Figure 6a displays the GISAXS profiles of the P3HT-RM/PCBM blend films treated at 150 °C for t = 0, 10, 30, and 240 min. According to our previous study[14] and the other report,[30] the main broad peak of GISAXS profiles at ~0.025 Å^{-1} increases due to the spherical PCBM aggregation clusters formed by the aggregation of PCBM molecules. The size of the PCBM clusters corresponding to this peak is 10−20 nm. The low-Q intensity upturn (0.003−0.01 Å^{-1}) was due to a larger phase, the so-called PCBM/P3HT amorphous domain,[27,31] rather than to the nanoscale clusters. This domain is composed of amorphous P3HT chains intercalated with PCBM molecules. According to a previous study,[23] this upturn intensity is increased by the scattering contrast because many PCBM molecules are dispersed in the amorphous polymer domains. We can determine the characteristic length, an approximate index of the PCBM/P3HT amorphous domain, by the Debye−Anderson−Brumberger (DAB) model using the GISAXS intensity, as shown in other studies.[24,25] To determine the respective structures of both

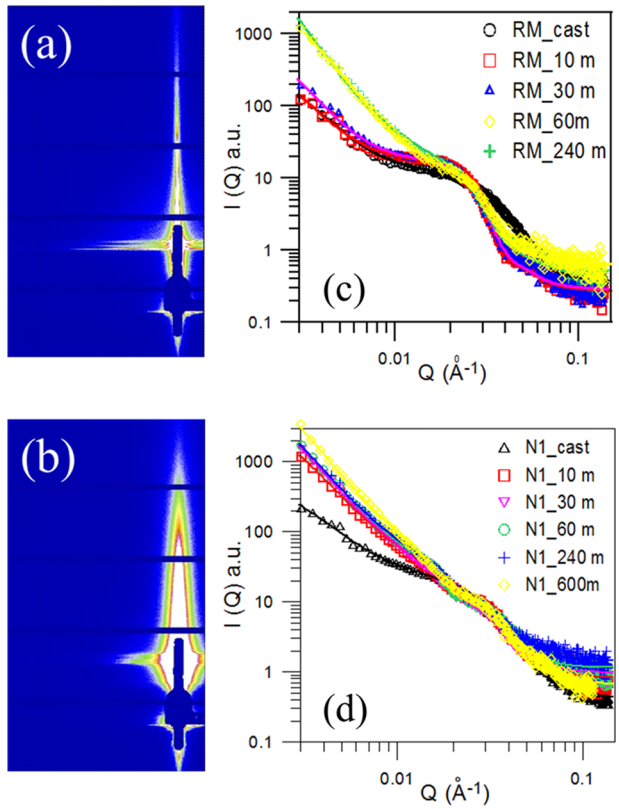

Figure 6. GISAXS patterns of the (a) as-cast P3HT-RM:PCBM film and (b) P3HT-RM:PCBM film treated at 150 °C for 240 min. In-plane GISAXS profiles of the (c) P3HT-RM:PCBM blend films and (d) P3HT-N1:PCBM blend films treated at 150 °C for various time intervals.

PCBM clusters and PCBM/P3HT amorphous domain, the GISAXS profiles can be expressed[25,31] as eqs 1 and 2.

$$I(Q) = \frac{A}{[1 + (Q\xi)^2]^2} + \eta V(\Delta\rho)^2 \left[\int_0^\infty F_i^2(Q, \sigma_i) f(\sigma_i) \mathrm{d}\sigma_i + \int_0^\infty \int_0^\infty F_i(Q, \sigma_i) F_j(Q, \sigma_j) H_{ij}(Q, \sigma_i, \sigma_j) f_i(\sigma_i) f_j(\sigma_j) \mathrm{d}\sigma_i \, \mathrm{d}\sigma_j \right] \quad (1)$$

$$F_i(Q, \sigma_i) = 4\pi \left(\sin(Q\sigma_i/2) - \frac{1}{2} Q\sigma_i \cos(Q\sigma_i/2) \right) \quad (2)$$

DOI: 10.1021/acsami.9b12482
ACS Appl. Mater. Interfaces 2019, 11, 40310−40319

where ξ is the characteristic length of the PCBM/P3HT amorphous domain described by the DAB model, and constant A is related to the product of $\Delta\rho$ and ξ^3. $\Delta\rho$ is the scattering length density contrast between the cluster and matrix. The model describing the PCBM clusters assumes that the clusters have a Schultz size distribution and a hard-sphere interaction between PCBM clusters. V is the average cluster volume. $F(Q, \sigma_I)^2$ is the form factor describing a spherical PCBM cluster of diameter σ_i. $H(Q, \sigma_i, \sigma_j)$ is the pair structure function describing the hard-sphere interaction.[32] The fitting parameters, η, R, and p, are the volume fraction, mean radius, and polydispersity of the Schultz size distribution.

All measured GISAXS profiles are well fitted by eq 1, as shown in Figure 6. The parameters, η, A, ξ, R, and p, determined by the model fitting are shown in Table 1. For the P3HT-RM:PCBM blend films, upon thermal annealing (from t = 0 to 10 min), the position of the broad peak corresponding to PCBM clusters began to shift toward the low-Q region, and the intensity increased. Therefore, there is an increase in the cluster radius and the corresponding volume fraction, suggesting the formation of an optimum BHJ structure. The fitted radii grow from 5.1 nm (as-cast) to 9.6 nm (t = 10 min). The fitted values of the volume fraction of PCBM clusters significantly increase from 3.2 to 16.5%. Note that the determined η values are relative values normalized to a reference value. That is because the fitted values of scattering contrast cannot be precisely measured and can be affected by some uncertainties, such as the penetration path. The variation of broad peaks of the GISAXS profiles (of Figure 6a) remains relatively stable from 10 to 240 min (fitted R values: ~10 nm, see Table 1), suggesting that the nanoscale PCBM cluster size is almost stable during the prolonged annealing. The corresponding volume fraction of clusters slightly increases from 16.5% (optimum BHJ structure) to 22.0% (thermally unstable at t = 240 min). It can be concluded that the temporal variations of growth and volume fraction of PCBM clusters attain saturation behavior of nanoscale PCBM aggregation predicted by the Avrami equation, even though the macroscale phase separation transits to the unstable stage. The values are consistent with the previously reported independent GISAXS results.[14] Note that the low-Q intensity upturn of the GISAXS profile corresponding to the mesoscale (defined here as around 40−200 nm) PCBM/P3HT amorphous domain gradually increases with time. The fitted values corresponding to the amorphous domains (approximated by characteristic length, ξ) are also listed in Table 1. This evolutional behavior is consistent with that previously reported.[14] The size of the mesoscale PCBM/P3HT amorphous domain remarkably increases from 48.9 nm for t = 30 min to 83.6 nm for t = 240 min, as indicated by the sharply increasing slope of the low-Q intensity upturn of Figure 6a. The concurrently rapid increase in constant A signifies the increase in the number of PCBM molecules in the amorphous domain. Similar cases were discussed in previous studies.[14,25] Compared to the nanoscale PCBM clusters, we defined this larger PCBM/P3HT amorphous domain as the mesoscale structure (Table 1). During the thermally unstable state, the noticeable growth and PCBM richness of these amorphous domains demonstrate an independent mesoscale phase separation.[14] In the meantime,

Table 1. Structural Parameters Determined by GISAXS Model Fitting and GIWAXS Peak Analysis for P3HT-RM and -N1:PCBM Blend Films Treated at 150 °C for Different Times

donor	t (min)	η (%)	R (nm)	p	A ($\times 10^{-5}$)	ξ (nm)	normalized crystallinity
P3HT-RM	0	3.2	5.1	0.29	1.27	34.4	28.51
	10	16.5	9.6	0.23	1.09	42.6	64.53
	30	18.7	9.8	0.26	1.71	48.9	66.97
	60	22.0	9.0	0.36	10.6	42.4	62.53
	240	22.0	9.4	0.45	13.4	83.6	186.03
P3HT-N1	0	2.9	3.1	0.12	2.5	29.9	40.26
	10	21.6	5.0	0.70	10.1	42.5	124.23
	30	20.7	4.9	0.76	12.4	51.2	126.60
	60	18.9	5.1	0.70	13.8	50.1	144.97
	240	17.9	5.5	0.70	13.5	53.0	115.48
	600	23.2	5.5	0.85	24.4	63.4	

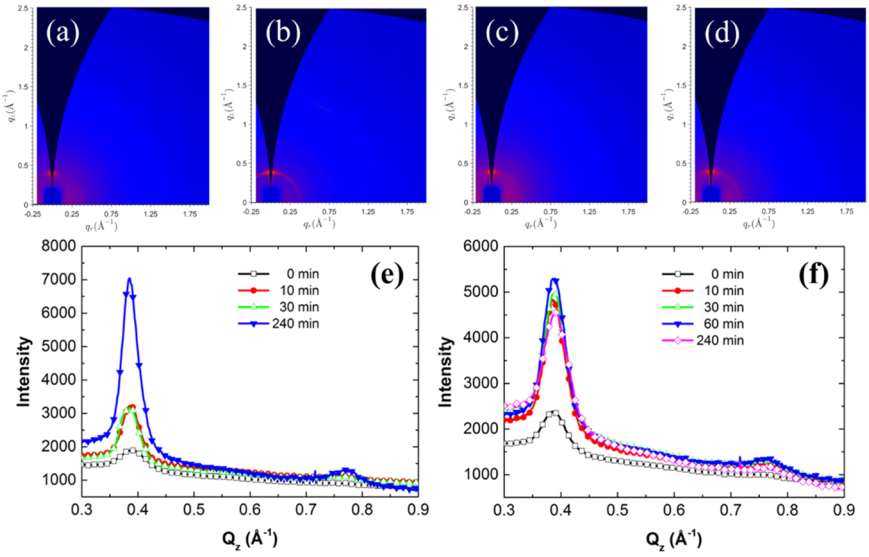

Figure 7. Two-dimensional GIWAXS patterns for P3HT-RM films treated at 150 °C for (a) 0 min, (b) 240 min, and P3HT-N1 blend films annealed at 150 °C for (c) 0 min, (d) 240 min. Temporal variations in the GIWAXS profiles of the (e) P3HT-RM and (f) P3HT-N1 blend films treated at 150 °C for various time intervals.

DOI: 10.1021/acsami.9b12482
ACS Appl. Mater. Interfaces 2019, 11, 40310−40319

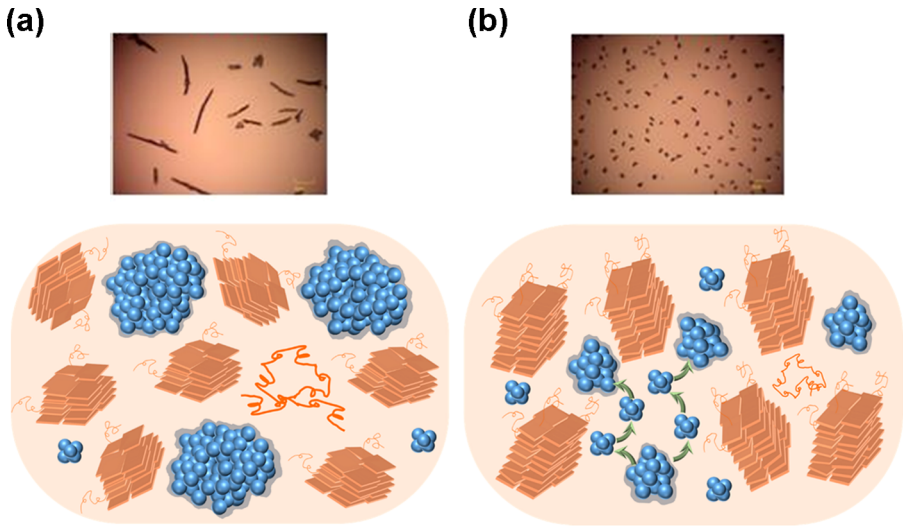

Figure 8. Schematics of the nanostructures of the devices based on (a) P3HT-RM:PCBM and (b) P3HT-N1:PCBM.

this process causes the formation of the same mesoscale PCBM-depleted (or P3HT-rich) domains due to the balance of molecules. The evolution of these mesoscale PCBM-depleted domains is intimately associated with the coincident formation of microscale PCBM-rich segregation (>10 μm; defined as the macroscale structure here). These macrodomains can be observed in the OM images. However, the mesoscale P3HT-rich and PCBM-rich domains and their significant variation with annealing time (revealed by the GISAXS technique) are difficult to identify in the corresponding TEM images (Figure 3a).

A previous research reported that the interaction between thermal motion of polymer chains and the $\pi-\pi$ interaction of C_{60} units may generate mesoscale PCBM-rich amorphous domains.[14] They would further coalesce into macroscale domains or aggregates under long-term thermal annealing. The remarkable reduction in the PCE starting from t = 60 min (Figure 6a and Table 1) agrees with the dramatic growth of the mesoscale P3HT-rich and PCBM-rich domains revealed by the GISAXS result. On the other hand, the corresponding OM images consistently show the formation and growth behavior of macroscale domains (Figure 2a). The independent GISAXS study for P3HT-RM:PCBM blend films also shows that the thermal instability and degraded PCE result from the dramatic variation of mesoscale P3HT/PCBM domains (also related to the concurrent formation and development of macroscale PCBM segregation) rather than the stable nanoscale PCBM clusters (related to the initial optimum BHJ structure). Both phase separations at the nanoscale and meso-/macroscale are almost independent of each other during the evolution from the optimum BHJ to the thermally unstable structure.

The GISAXS profiles of the P3HT-N1:PCBM blend films treated at 150 °C for 0, 10, 30, 60, and 240 min are shown in Figure 6b to investigate the excellent thermal stability. According to the fitting result (Table 1), the radius of PCBM clusters in the as-cast P3HT-N1:PCBM film (3.1 nm) is lower than that in the as-cast P3HT-RM:PCBM film (5.1 nm). The values suggest that the P3HT-N1:PCBM blend film decreases the size of PCBM clusters during the formation of the initial phase-separated BHJ structure. Consistently, the GIWAXS profiles (discussed later; Figure 7) show that the P3HT-N1 blend film has relatively higher polymer crystallinity than those based on P3HT-RM. It can be concluded, then, that the large amount of nanoscale P3HT crystallites and their spatial dispersion in the amorphous domain (due to the molecular RR) confine the molecular diffusion, nucleation, and growth of the PCBM cluster, reducing the cluster size. The growth of PCBM clusters after thermal annealing at 150 °C (R = 5.0 nm at t = 10 min) is also confined compared to that of the annealed P3HT-RM:PCBM blend film ($R \sim$ 10 nm). The size of PCBM clusters for the annealed P3HT-N1:PCBM blend films remains stable during the prolonged annealing, which is similar to the temporal behavior of nanoscale PCBM clusters in the annealed P3HT-RM:PCBM blend film. Overall, the fitted values of the volume fraction of PCBM clusters for both the annealed P3HT-N1 and -RM:PCBM blend films are similar, ~20%, and remain stable from 10 to 600 min.

Because the volume fraction is the product of cluster number density and cluster volume, the number density of PCBM clusters of the P3HT-N1-base blend film is much higher than that of the P3HT-RM-base blend film. This factor can lead to (1) a high interface area between PCBM clusters and the P3HT phase at the nanoscale (favorable to charge separation) and (2) a uniform spatial dispersion of PCBM clusters or network connected by PCBM clusters (favorable to the charge transport; the charge carriers can hop between PCBM clusters). The performance of the P3HT-N1:PCBM devices remained relatively stable (above 80% of the initial PCE) during the prolonged annealing up to 760 min. This can be directly correlated with the invariance or thermal stability of the mesoscale PCBM/P3HT amorphous domains quantitatively revealed by the GISAXS study (Table 1). According to a previous study, the mesoscale domain partly contributes to the performance because it is also favorable to the charge separation and transport on the molecular scale.[14] This result confirms that an effective approach to suppress thermal instability and degradation of PCE is to inhibit the coalescence of the meso- into the large-scale PCBM/P3HT amorphous domains. According to the A values of Table 1 (related to the PCBM molecules in the mesoscale domains), the much higher density of PCBM molecules particularly distributed or intercalated by the molecular chain in the mesoscale domains is not affected by the prolonged annealing, explaining why only the P3HT-N1:PCBM films have small and well-dispersed macroscale PCBM segregation (thermally stable dots observed by OM).

DOI: 10.1021/acsami.9b12482
ACS Appl. Mater. Interfaces 2019, 11, 40310−40319

These dots are unlike the local and large segregation observed in the usual (or P3HT-RM-based) case.

The temporal variations of 1D GIWAXS profiles of the annealed P3HT-RM and P3HT-N1 blend films, corresponding to the simultaneous GISAXS measurements (Figure 6), are shown in Figure 7. Compared to the 1D GIWAXS profiles contributed by edge-on, face-on, and all-orientation P3HT crystallites and 2D GIWAXS patterns, the relative P3HT crystallinity can be roughly determined by the integrated peak intensity of the (100) peak from the dominated edge-on P3HT lamellar structure, similar to the previous study.[33] The relatively normalized crystallinity for both blend films is listed in Table 1. The evolution of GIWAXS profiles with heating time provides evidence that the polymer with high RR easily crystallizes during casting and heating. After heating for 10 min, the crystallinity development of the P3HT-N1 blend film almost saturates, and there is no significant increase in relative crystallinity even after 240 min of heating. These results indicate that the P3HT-N1 crystallinity is relatively stable over a long heating time. In contrast, the P3HT-RM blend film (low RR) shows growing crystallinity with increasing heating time. The unstable crystallinity behavior implies that severe phase separation between P3HT and PCBM will occur with long annealing time. Therefore, the P3HT-N1 blend film shows better thermal stability than the P3HT-RM blend film. This may be partly due to the mutual confinement between the well-dispersed PCBM clusters and the nanoscale P3HT crystallites. The differences between polymer regioregularities could lead to a distinctive polymer crystallization and spatial distribution, and thus tailor the PCBM cluster size and distribution. Moreover, the meso- and micron-scale phase-separated structures can facilitate thermal stability. The nanoscale BHJ structure can enhance the PCE. From the GIWAXS and GISAXS analysis, the nanostructures of devices consisting of P3HT-RM and P3HT-N1 under long annealing time are illustrated schematically in Figure 8.

Some earlier works by Swinnen and Manca et al.[34−40] intensively studied the structural evolution of PCBM needlelike crystals in a heated polymer/PCBM blend by various microscopies, including atomic force microscopy, TEM, selected-area electron diffraction analysis, OM, and confocal fluorescence microscopy. The growth mechanism of PCBM and P3HT phases proposed by these research studies can be consistently incorporated to provide a complementary interpretation of GISAXS and GIWAXS results. Based on the mechanistic insight combining various characterizations at different length scales during heating of the blend, the phase-separation mechanism for tuning the spatial distribution and growth (or crystallization) of PCBM and P3HT crystallites by the regioregularity is described as follows. In the initial period of PCBM and P3HT crystallization during the casting of the blend film, the P3HT crystallization of faster kinetics governs the formation, size, and distribution of PCBM clusters followed by the formation of the other-scale P3HT/PCBM amorphous domains. The kinetics of P3HT crystallization depends on the mixing conditions of the blend.[41] However, the mutual hindrance or confinement between the growths of P3HT and PCBM structures becomes important after nuclei formation during prolonged heat treatment.[14,23,27]

For the P3HT-RM case with rather lower level of regioregularity, the uniformly distributed P3HT-RM molecules in the amorphous matrix crystallize more slowly than the P3HT-N1 molecules with high regioregularity, as reported by GIWAXS. The P3HT-N1 molecules in the blend may have more local, relatively high concentration regions in which the nearby PCBM-molecule-rich regions also concurrently form, as evidenced by GISAXS (Table 1). This situation leads to the formation of more P3HT-N1 crystallite nuclei and fast P3HT-N1 crystallization kinetics. In contrast, P3HT-RM crystallites in the blend have few nuclei, and thus they mainly grow with thermal heating. The growth of large-scale P3HT-RM crystallites could cause the expulsion of a large number of PCBM molecules into the amorphous domains, leading to the locally high concentration of PCBM molecules in the amorphous domains (consisting of several mesoscale P3HT/PCBM domains). With prolonged heating, the thermal aggregation of PCBM molecules will enable the coalescence of several mesoscale amorphous domains into microsized PCBM-rich segregation (i.e., needlelike PCBM crystallites in the OM image). The structural details and mechanism are also described in the literature.[34−40] On the other hand, the dense distribution of small P3HT-N1 crystallites (growth from nuclei) leads to a large number of small PCBM nanoscale clusters and their network-like distribution due to the mutual hindrance between them. The network of nanoscale PCBM clusters will further restrict the development of mesoscale domains into the large microsized PCBM-rich domains. It is evidenced here (GISAXS analysis) that the thermal diffusion of PCBM molecules is limited within the mesoscale domains during the prolonged heating.

CONCLUSION

In conclusion, we have shown that the multilength-scale formation of PCBM aggregation greatly influences the thermal stability of PSCs. Devices prepared with both high- and low-RR polymers exhibit large PCBM aggregates on a macroscale; however, they have completely different thermal stability behaviors. We determined that the thermal stability of PSCs is highly related to the mesoscale PCBM/P3HT amorphous domain, and that the domain growth into large-scale size should be prevented. In addition, we demonstrated that the P3HT-N1:PCBM blend films tend to form some small crystallites and lead to higher interaction between P3HT-N1 crystallites and PCBM clusters, resulting in better thermal behavior compared to PSCs based on P3HT-RM:PCBM blend films. Our GISAXS/GIWAXS study provides mechanistic insight to understand how the PCBM formation on the multilength scale affects the evolution of the nanostructures related to the thermal stability of P3HT-based PSCs.

ASSOCIATED CONTENT

Supporting Information

The Supporting Information is available free of charge on the ACS Publications website at DOI: 10.1021/acsami.9b12482.

Regioregularity and NMR spectra for different polymers (Figure S1); full $J-V$ plots (Figure S2); and related photovoltaic characteristics (Table S1) (PDF)

AUTHOR INFORMATION

Corresponding Authors

*E-mail: huangyc@mail.mcut.edu.tw (Y.-C.H.).
*E-mail: cstsao@iner.gov.tw (C.-S.T.).
*E-mail: leewang@ntu.edu.tw (L.W.).

ORCID

Yu-Ching Huang: 0000-0003-4772-8050

DOI: 10.1021/acsami.9b12482
ACS Appl. Mater. Interfaces 2019, 11, 40310−40319

Leeyih Wang: 0000-0002-6368-0141

Notes

The authors declare no competing financial interest.

■ ACKNOWLEDGMENTS

The authors would like to thank Wei-Ru Wu for correcting GIWAXS patterns by pole figure reconstruction. This work was financially supported by the Ministry of Science and Technology (MOST 105-2119-M-002-030-MY3; MOST 107-2218-E-131-007), Academia Sinica (AS-106-SS-A02; 2394-106-0300), and the Center of Atomic Initiative for New Materials, National Taiwan University, through the Featured Areas Research Center Program within the framework of the Higher Education Sprout Project by the Ministry of Education, Taiwan.

■ REFERENCES

(1) Nielsen, T. D.; Cruickshank, C.; Foged, S.; Thorsen, J.; Krebs, F. C. Business, Market and Intellectual Property Analysis of Polymer Solar Cells. *Sol. Energy Mater. Sol. Cells* **2010**, *94*, 1553−1571.

(2) Espinosa, N.; Hosel, M.; Jorgensen, M.; Krebs, F. C. Large Scale Deployment of Polymer Solar Cells on Land, on Sea and in The Air. *Energy Environ. Sci.* **2014**, *7*, 855−866.

(3) Huang, Y.-C.; Cha, H.-C.; Chen, C.-Y.; Tsao, C.-S. A Universal Roll-to-roll Slot-die Coating Approach towards High-efficiency Organic Photovoltaics. *Prog. Photovolt: Res. Appl.* **2017**, *25*, 928−935.

(4) Liu, H.-W.; Chang, D.-Y.; Chiu, W.-Y.; Rwei, S.-P.; Wang, L. Fullerene Bisadduct as An Effective Phase-Separation Inhibitor in Preparing Poly(3-Hexylthiophene)-[6,6]-Phenyl-C61-Butyric Acid Methyl Ester Blends with Highly Stable Morphology. *J. Mater. Chem.* **2012**, *22*, 15586−15591.

(5) Diacon, A.; Derue, L.; Lecourtier, C.; Dautel, O.; Wantz, G.; Hudhomme, P. Cross-linkable Azido C60-fullerene Derivatives for Efficient Thermal Stabilization of Polymer Bulk-heterojunction Solar Cells. *J. Mater. Chem. C* **2014**, *2*, 7163−7167.

(6) Morse, G. E.; Tournebize, A.; Rivaton, A.; Chassé, T.; Taviot-Gueho, C.; Blouin, N.; Lozman, O. R.; Tierney, S. The Effect of Polymer Solubilizing Side-chains on Solar Cell Stability. *Phys. Chem. Chem. Phys.* **2015**, *17*, 11884−11897.

(7) Li, Z.; Wu, F.; Lv, H.; Yang, D.; Chen, Z.; Zhao, X.; Yang, X. Side-chain Engineering for Enhancing the Thermal Stability of Polymer Solar Cells. *Adv. Mater.* **2015**, *27*, 6999−7003.

(8) Heckler, I.; Kesters, J.; Defour, M.; Madsen, V. M.; Penxten, H.; D'Haen, J.; Van Mele, B.; Maes, W.; Bundgaard, E. The Influence of Conjugated Polymer Side Chain Manipulation on the Efficiency and Stability of Polymer Solar Cells. *Materials* **2016**, *9*, 181.

(9) Vandenbergh, J.; Conings, B.; Bertho, S.; Kesters, J.; Spoltore, D.; Esiner, S.; Zhao, J.; Van Assche, G.; Wienk, M. M.; Maes, W.; Lutsen, L.; Van Mele, B.; Janssen, R. A. J.; Manca, J.; Vanderzande, D. J. M. Thermal Stability of Poly[2-methoxy-5-(2′-phenylethoxy)-1,4-phenylenevinylene] (MPE-PPV):fullerene Bulk Heterojunction Solar Cells. *Macromolecules* **2011**, *44*, 8470−8478.

(10) Campo, B. J.; Bevk, D.; Kesters, J.; Gilot, J.; Bolink, H. J.; Zhao, J.; Bolsée, J.-C.; Oosterbaan, W. D.; Bertho, S.; D'Haen, J.; Manca, J.; Lutsen, L.; Van Assche, G.; Maes, W.; Janssen, R. A. J.; Vanderzande, D. Ester-functionalized Poly(3-alkylthiophene) Copolymers: Synthesis, Physicochemical Characterization and Performance in Bulk Heterojunction Organic Solar Cells. *Org. Electron.* **2013**, *14*, 523−534.

(11) Kesters, J.; Verstappen, P.; Raymakers, J.; Vanormelingen, W.; Drijkoningen, J.; D'Haen, J.; Manca, J.; Lutsen, L.; Vanderzande, D.; Maes, W. Enhanced Organic Solar Cell Stability by Polymer (PCPDTBT) Side Chain Functionalization. *Chem. Mater.* **2015**, *27*, 1332−1341.

(12) Miyanishi, S.; Tajima, K.; Hashimoto, K. Morphological Stabilization of Polymer Photovoltaic Cells by Using Cross-linkable Poly(3-(5-hexenyl)thiophene). *Macromolecules* **2009**, *42*, 1610−1618.

(13) Rumer, J. W.; McCulloch, I. Organic Photovoltaics: Crosslinking for Optimal Morphology and Stability. *Mater. Today* **2015**, *18*, 425−435.

(14) Chen, C.-Y.; Tsao, C.-S.; Huang, Y.-C.; Liu, H.-W.; Chiu, W.-Y.; Chuang, C.-M.; Jeng, U. S.; Su, C.-J.; Wu, W.-R.; Su, W.-F.; Wang, L. Mechanism and Control of Structural Evolution of Polymer Solar Cell from Bulk Heterojunction to Thermally Unstable Hierarchical Structure. *Nanoscale* **2013**, *5*, 7629−7638.

(15) Huang, Y.-C.; Liao, Y.-C.; Li, S.-S.; Wu, M.-C.; Chen, C.-W.; Su, W.-F. Study of The Effect of Annealing Process on The Performance of P3HT/PCBM Photovoltaic Devices Using Scanning-probe Microscopy. *Sol. Energy Mater. Sol. Cells* **2009**, *93*, 888−892.

(16) Li, G.; Yao, Y.; Yang, H.; Shrotriya, V.; Yang, G.; Yang, Y. "Solvent Annealing" Effect in Polymer Solar Cells Based on Poly(3-hexylthiophene) and Methanofullerenes. *Adv. Funct. Mater.* **2007**, *17*, 1636−1644.

(17) De Sio, A.; Madena, T.; Huber, R.; Parisi, J.; Neyshtadt, S.; Deschler, F.; Da Como, E.; Esposito, S.; von Hauff, E. Solvent Additives for Tuning The Photovoltaic Properties of Polymer−fullerene Solar Cells. *Sol. Energy Mater. Sol. Cells* **2011**, *95*, 3536−3542.

(18) Kim, Y.; Cook, S.; Tuladhar, S. M.; Choulis, S. A.; Nelson, J.; Durrant, J. R.; Bradley, D. D. C.; Giles, M.; McCulloch, I.; Ha, C.-S.; Ree, M. A Strong Regioregularity Effect in Self-organizing Conjugated Polymer Films And High-Efficiency Polythiophene:Fullerene Solar Cells. *Nat. Mater.* **2006**, *5*, 197−203.

(19) Li, G.; Shrotriya, V.; Yao, Y.; Huang, J.; Yang, Y. Manipulating Regioregular Poly(3-hexylthiophene): [6,6]-Phenyl-C61-Butyric Acid Methyl Ester Blends—Route towards High Efficiency Polymer Solar Cells. *J. Mater. Chem.* **2007**, *17*, 3126−3140.

(20) Sun, J.-P.; Blaskovits, J. T.; Bura, T.; Beaupré, S.; Leclerc, M.; Hill, I. G. Photovoltaic Device Performance of Highly Regioregular Fluorinated Poly(3-hexylthiophene). *Org. Electron.* **2017**, *50*, 115−120.

(21) Chuang, S.-Y.; Chen, H.-L.; Lee, W.-H.; Huang, Y.-C.; Su, W.-F.; Jen, W.-M.; Chen, C.-W. Regioregularity Effects in The Chain Orientation and Optical Anisotropy of Composite Polymer/fullerene Films for High-efficiency, Large-area Organic Solar Cells. *J. Mater. Chem.* **2009**, *19*, 5554−5560.

(22) Sivula, K.; Luscombe, C. K.; Thompson, B. C.; Fréchet, J. M. J. Enhancing the Thermal Stability of Polythiophene:fullerene Solar Cells by Decreasing Effective Polymer Regioregularity. *J. Am. Chem. Soc.* **2006**, *128*, 13988−13989.

(23) Huang, Y.-C.; Tsao, C.-S.; Chuang, C.-M.; Lee, C.-H.; Hsu, F.-H.; Cha, H.-C.; Chen, C.-Y.; Lin, T.-H.; Su, C.-J.; Jeng, U. S.; Su, W.-F. Small- and Wide-Angle X-ray Scattering Characterization of Bulk Heterojunction Polymer Solar Cells with Different Fullerene Derivatives. *J. Phys. Chem. C* **2012**, *116*, 10238−10244.

(24) Liao, H.-C.; Tsao, C.-S.; Shao, Y.-T.; Chang, S.-Y.; Huang, Y.-C.; Chuang, C.-M.; Lin, T.-H.; Chen, C.-Y.; Su, C.-J.; Jeng, U. S.; Chen, Y.-F.; Su, W.-F. Bi-hierarchical Nanostructures of Donor-Acceptor Copolymer and Fullerene for High Efficient Bulk Heterojunction Solar Cells. *Energy Environ. Sci.* **2013**, *6*, 1938−1948.

(25) Huang, Y.-C.; Tsao, C.-S.; Cha, H.-C.; Chuang, C.-M.; Su, C.-J.; Jeng, U. S.; Chen, C.-Y. Correlation between Hierarchical Structure and Processing Control of Large-area Spray-coated Polymer Solar Cells toward High Performance. *Sci. Rep.* **2016**, *6*, No. 20062.

(26) Chen, W.; Nikiforov, M. P.; Darling, S. B. Morphology Characterization in Organic and Hybrid Solar Cells. *Energy Environ. Sci.* **2012**, *5*, 8045−8074.

(27) Liao, H.-C.; Tsao, C.-S.; Lin, T.-H.; Jao, M.-H.; Chuang, C.-M.; Chang, S.-Y.; Huang, Y.-C.; Shao, Y.-T.; Chen, C.-Y.; Su, C.-J.; Jeng, U. S.; Chen, Y.-F.; Su, W.-F. Nanoparticle-tuned Self-organization of a Bulk Heterojunction Hybrid Solar Cell with Enhanced Performance. *ACS Nano* **2012**, *6*, 1657−1666.

(28) Guo, S.; Wang, W.; Herzig, E. M.; Naumann, A.; Tainter, G.; Perlich, J.; Müller-Buschbaum, P. Solvent−morphology−property Relationship of PTB7:$PC_{71}BM$ Polymer Solar Cells. *ACS Appl. Mater. Interfaces* **2017**, *9*, 3740−3748.

(29) Guo, S.; Ning, J.; Körstgens, V.; Yao, Y.; Herzig, E. M.; Roth, S. V.; Müller-Buschbaum, P. The Effect of Fluorination in Manipulating

DOI: 10.1021/acsami.9b12482
ACS Appl. Mater. Interfaces 2019, 11, 40310−40319

the Nanomorphology in PTB7:$PC_{71}BM$ Bulk Heterojunction Systems. *Adv. Energy Mater.* **2015**, *5*, No. 1401315.
(30) Chen, W.; Xu, T.; He, F.; Wang, W.; Wang, C.; Strzalka, J.; Liu, Y.; Wen, J.; Miller, D. J.; Chen, J.; Hong, K.; Yu, L.; Darling, S. B. Hierarchical Nanomorphologies Promote Exciton Dissociation in Polymer/Fullerene Bulk Heterojunction Solar Cells. *Nano Lett.* **2011**, *11*, 3707−3713.
(31) Liao, H.-C.; Tsao, C.-S.; Lin, T.-H.; Chuang, C.-M.; Chen, C.-Y.; Jeng, U. S.; Su, C.-H.; Chen, Y.-F.; Su, W.-F. Quantitative Nano-organized Structural Evolution for A High Efficiency Bulk Heterojunction Polymer Solar Cell. *J. Am. Chem. Soc.* **2011**, *133*, 13064−13073.
(32) Griffith, W. L.; Triolo, R.; Compere, A. L. Analytical Scattering Function of A Polydisperse Percus-Yevick Fluid with Schulz- (Gamma-) Distributed Diameters. *Phys. Rev. A* **1987**, *35*, 2200−2206.
(33) González, D. M.; Schaffer, C. J.; Pröller, S.; Schlipf, J.; Song, L.; Bernstorff, S.; Herzig, E. M.; Müller-Buschbaum, P. Codependence between Crystalline and Photovoltage Evolutions in P3HT:PCBM Solar Cells Probed with in-Operando GIWAXS. *ACS Appl. Mater. Interfaces* **2017**, *9*, 3282−3287.
(34) Zhao, J.; Swinnen, A.; Van Assche, G.; Manca, J.; Vanderzande, D.; Mele, B. V. Phase Diagram of P3HT/PCBM Blends and Its Implication for the Stability of Morphology. *J. Phys. Chem. B* **2009**, *113*, 1587−1591.
(35) Mens, R.; Adriaensens, P.; Lutsen, L.; Swinnen, A.; Bertho, S.; Ruttens, B.; D'Haen, J.; Manca, J.; Cleij, T.; Vanderzande, D.; Gelan, J. NMR Study of The Nanomorphology in Thin Films of Polymer Blends Used in Organic PV Devices: MDMO-PPV/PCBM. *J. Polym. Sci., Part A: Polym. Chem.* **2008**, *46*, 138−145.
(36) Bertho, S.; Haeldermans, I.; Swinnen, A.; Moons, W.; Martens, T.; Lutsen, L.; Vanderzande, D.; Manca, J.; Senes, A.; Bonfiglio, A. Influence of Thermal Ageing on The Stability of Polymer Bulk Heterojunction Solar Cells. *Sol. Energy Mater. Sol. Cells* **2007**, *91*, 385−389.
(37) Douhéret, O.; Swinnen, A.; Bertho, S.; Haeldermans, I.; D'Haen, J.; D'Olieslaeger, M.; Vanderzande, D.; Manca, J. V. High-resolution Morphological and Electrical Characterisation of Organic Bulk Heterojunction Solar Cells by Scanning Probe Microscopy. *Prog. Photovoltaics: Res. Appl.* **2007**, *15*, 713−726.
(38) Swinnen, A.; Haeldermans, I.; vande Ven, M.; D'Haen, J.; Vanhoyland, G.; Aresu, S.; D'Olieslaeger, M.; Manca, J. Tuning the Dimensions of C_{60}-Based Needlelike Crystals in Blended Thin Films. *Adv. Funct. Mater.* **2006**, *16*, 760−765.
(39) Vanlaeke, P.; Swinnen, A.; Haeldermans, I.; Vanhoyland, G.; Aernouts, T.; Cheyns, D.; Deibel, C.; D'Haen, J.; Heremans, P.; Poortmans, J.; Manca, J. V. P3HT/PCBM Bulk Heterojunction Solar Cells: Relation between Morphology and Electro-Optical Characteristics. *Sol. Energy Mater. Sol. Cells* **2006**, *90*, 2150−2158.
(40) Goris, L.; Poruba, A.; Purkrt, A.; Vandewal, K.; Swinnen, A.; Haeldermans, I.; Haenen, K.; Manca, J.; Vanecek, M. Optical Absorption by Defect States in Organic Solar Cells. *J. Non-Cryst. Solids* **2006**, *352*, 1656−1659.
(41) Wu, W.-R.; Jeng, U.-S.; Su, C.-J.; Wei, K.-H.; Su, M.-S.; Chiu, M.-Y.; Chen, C.-Y.; Su, W.-B.; Su, C.-H.; Su, A.-C. Competition between Fullerene Aggregation and Poly(3-hexylthiophene) Crystallization upon Annealing of Bulk Heterojunction Solar Cells. *ACS Nano* **2011**, *5*, 6233−6243.

DOI: 10.1021/acsami.9b12482
ACS Appl. Mater. Interfaces 2019, 11, 40310−40319